Constructing dendrite suppressing mixed sulfide solid electrolyte for high-rate lithium metal batteries

Z. Ge, S.N. Chen, R. Wang, R Ma, B. Fan, D. Le Coq, X. Zhang, H. Ma, B. Xue

Constructing dendrite suppressing mixed sulfide solid electrolyte for high-rate lithium metal batteries

Zeyu Ge[a,b,c&], Nanshan Chen[a&], Rui Wang[a], Rui Ma[b], Bo Fan[a], David Le coq[c], Xianghua Zhang[c], Hongli Ma[c], and Bai Xue[a]*

[a] *Shenzhen Key Laboratory of Advanced Thin Films and Applications, College of Physics and Optoelectronic Engineering, Shenzhen University, Shenzhen, 518060, China*

[b] *College of Chemistry and Environmental Engineering, Shenzhen University, Shenzhen, 518060, China*

[c] *Univ Rennes, CNRS, ISCR (Institut des Sciences Chimiques de Rennes) – UMR 6226, Rennes 35042, France*

[&] These authors contributed equally to this work as co-first authors.

* Corresponding author. E-mail address: baixue@szu.edu.cn

Keywords: dendrite-free, interface, composite structure, solid-state electrolyte

ABSTRACT

All-solid-state lithium metal batteries (ASSLMBs) have received much attention because of their potential for high energy density and high safety performance. However, the poor compatibility of the lithium/solid electrolytes (SEs) interface and the penetration of lithium dendrites during cycling prevent them from achieving current densities that are capable of commercialization. In this work, a lithium-metastable solid electrolyte and a lithium-unstable solid electrolyte have been mixed to obtain mix-structured solid electrolyte. In particular, $Li_{5.5}PS_{4.5}Cl_{1.5}$ acts as a lithium-compatible matrix, and $Li_{10}SnP_2S_{12}$ as a dendrite-scavenger. The synergy between the two generates a stable interface with the Li anode and effectively suppresses the penetration of lithium dendrites. Li symmetric cells can operate stably for 160 h at a current density of 0.5 mA cm^{-2} at room temperature. The critical current density can reach 5 mA cm^{-2} and the overpotential is less than 0.5 V. The Li/SEs/$Li_4Ti_5O_{12}$ all-solid-state cells show a high capacity of 174 mAh g^{-1} at 0.2 C and 148 mAh g^{-1} at 2 C. High-capacity retentions of 97.3% and 94.4% are shown after 75 cycles at 1 C and 2 C at room temperature, respectively. This work highlights the advantages of the electrolyte with mixed structure and provides a new strategy to resist lithium dendrites and improve the critical current density and cycle life of ASSLMBs.

1. Introduction

Lithium-ion batteries have gained popularity as a method of energy storage due to their energy density of more than 250 Wh kg^{-1} and reasonable cost [1, 2]. However, further improvements in battery energy density have been severely constrained by the usage of conventional graphite anodes. Therefore, researchers are increasingly interested in the use of lithium metal anodes with 10 times the gravimetric capacity of graphite [3, 4]. On the other hand, the liquid electrolytes used in conventional batteries are usually flammable and unstable with the lithium metal anode. Solid electrolytes (SEs) have proven to be perfect for lithium metal anodes due to their durability at high temperatures and lack of concentration polarization [5-7]. All solid-state lithium metal batteries (ASSLMBs) are in the spotlight for the development of next-generation energy storage devices due to their non-flammability, non-leakage, high energy density, long cycle life, and high safety.

There is a key issue with the current application of solid-state electrolytes to ASSLMBs, i.e., most electrolytes still have a small critical current density (CCD) (< 0.5 mA cm^{-2}) to resist the lithium penetration which does not match the organic electrolytes (> 2 mA cm^{-2}) [8]. For example, the widely studied oxide solid electrolytes, such as the garnet-type $Li_7La_3Zr_2O_{12}$, have strong chemical stability, a wide range of electrochemical stability, and good stability with lithium metal [9, 10]. However, oxide electrolytes are typically brittle, have poor electrode/electrolyte interface contact, and usually need sintering at temperatures more than 1000°C. They also cannot be cold-pressed into form. Typically, their critical current densities are less than 0.5 mA cm^{-2} [11]. Due to their high ionic conductivity, sulfide electrolytes are widely used in all-solid-state batteries [12]. Nonetheless, the CCD of sulfide electrolytes is typically lower than 1 mA cm^{-2} even with $Li_{5.5}PS_{4.5}Cl_{1.5}$ (LPSCl), which has an ionic conductivity of up to 9.4 mS cm^{-1} [13, 14]. There is an urgent need to develop solid electrolytes with greater CCD that can suppress the formation of lithium dendrites.

Another significant problem is the interfacial compatibility of solid-state electrolytes with lithium metal. Most solid electrolytes have side reactions when they come into contact with lithium metal [15]. A thick mixed conducting interphase (MCI) layer forms in the electrolytes which contain the elements like Ge, Sn, and Si [16]. For instance, an interphase that includes ion-conduction phases (Li_3P) and electron-conduction phases (Li-Sn alloys) forms at the interface between $Li_{10}SnP_2S_{12}$ (LSPS) and lithium [17]. Calculations show that $Li_{10}GeP_2S_{12}$ (LGPS) is expected to undergo similar electrochemical reductions at voltages below 1.7 V [18]. Even though the LGPS has an ionic conductivity comparable to that of organic liquid electrolytes (12 mS cm^{-1}), the accumulation and thickening of these interphase layers significantly impede the transport of lithium ions across the interface [19, 20]. Lithium alloys like Li-In and Li-Al can presently be used to limit the growth of MCI layers [21]. However, the redox potential of Li-In electrodes is 0.62 V vs Li/Li^+, which significantly reduces the specific energy of the battery, and the high price of indium makes it almost impossible to industrialize [22].

For other solid electrolytes where the metastable solid electrolyte interphase (SEI) layer, rather than the rapidly thickening MCI layer, is formed in contact with Li metal, the compositional inhomogeneity of the interphase layer leads to uneven lithium deposition [14]. This phenomenon is partially mitigated by lithium diffusion and creep under appropriate pressure when the battery operates at a low current density [23, 24]. However, this phenomenon deteriorates when the current density increases, leading to

the penetration of lithium dendrites into the solid electrolytes and causing short circuits in all-solid-state cells. Thus, it is critical to developing novel solid electrolytes with a robust interface with lithium metal anodes.

In general, there are two failure modes related to interface problems between the solid electrolytes and the lithium metal anodes. In the first case, a stable SEI layer is formed. Lithium dendrites grow from the poorly contacted solid electrolyte/lithium interface, propagate through the grain/particle boundaries, and finally lead to a short circuit (e.g., Fig. 1a) [25]. In the second case, lithium forms an MCI layer with the electrolyte. Even though lithium does not penetrate the battery directly, the rapidly thickening MCI layer results in a huge interfacial resistance, and the battery fails owing to the excessive overpotential (Fig. 1b) [26]. The use of multilayer composite structures or composite electrolytes is an effective approach to solve these interface problems. Currently, some methods are used to form a protective layer on the electrolyte to prevent the electrolyte from reacting with Li to form an MCI layer. However, this protective layer can be further enhanced in terms of stability, maximum current density withstood, and complex preparation processes [27-29]. Other methods are the composite of inorganic solid electrolytes with polymer electrolytes (PEO, etc.) [30-33]. These methods can provide stable SE/Li interface, but typically require high operating temperature to achieve the desired ionic conductivity. High-performance composite solid electrolytes are vitally required.

An effective solid electrolyte has to fulfill the following criteria: (i) good stability with lithium metal and be free of a continually and rapidly expanding interfacial layer. (ii) high resistance to lithium dendrite even under a high current density to handle the high-rate performance of the battery. This study demonstrates that mixing two solid electrolytes with distinct properties using a straightforward grinding method can be an effective way to achieve the forementioned crtieria. This method makes use of two electrolytes, one of which is stable to lithium metal (LPSCl, etc.) and the other efficiently consumes lithium dendrites (LGPS, LSPS, etc.). The mixed solid electrolyte (MIX) can be prepared by simply hand-grinding the two electrolytes (Fig. 1c). This simple mixing does not change the physicochemical properties of the two electrolytes, but in a synergetic way they can preserve the good stability with lithium metal while eliminating the lithium dendrites. Trees often suffer injuries such as insect holes and felling wounds. If leaving these injuries untreated, the injury parts will expand and eventually damage the mechanical strength of the trunk. Naturally, the injuries stimulate the tree to form a healing shell around them, which prevents the expansion of the injury parts (Fig. S1). We believe that a similar self-healing mechanism also works for suppressing lithium dendrites in the MIX electrolytes. The dendrites which penetrate into the solid electrolyte will react locally with the Li-consuming electrolytes, forming a highly electrical resistive region to prevent the further growth of the dendrites. By using the mixed solid electrolytes, the lithium symmetric cell can operate at a current density of 5 mA cm^{-2}, and its overpotential at this current density is less than 0.5 V. Additionally, the rapid increase in interfacial resistance observed in cycles using only LSPS as the electrolyte is effectively suppressed when using the MIX electrolyte, indicating good stability with lithium metal. The overpotential increase of the mixed solid electrolyte is substantially slower than that of the conventional LSPS cell at the current of 0.5 mA cm^{-2} and remains steady for hundreds of hours. It is also demonstrated that the mixed solid electrolyte can guarantee the stable operation of a Li/SEs/ $Li_4Ti_5O_{12}$ (LTO) full battery at 2 C rate, which maintains 94% capacity after 75 cycles. The mixed

solid electrolyte combines the advantages of compatibility with lithium and inhibition of lithium dendrites. They are promising candidates for high-rate-operating ASSLMBs. Moreover, the synthesis method is simple to operate and easy to industrialize.

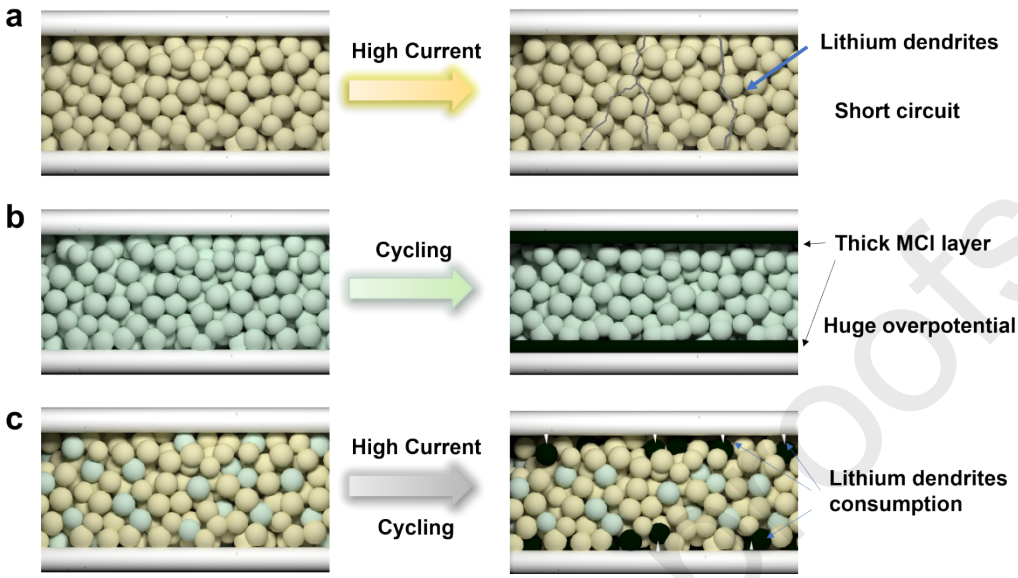

Figure 1. Using MIX electrolyte to alleviate the two failure modes associated with the solid electrolyte/Li interface. (a) Cell with stable interface, Li dendrite penetration occurs. (b) Cell with unstable interface, a continually growing interphase layer leads to a huge overpotential. (c) Cell with the MIX electrolyte. The unstable electrolyte reacts with the penetrated dendrites that impairs their growth, and the stable electrolyte acts as a stable ion-conductive matrix, guaranteeing a low effective electronic conductivity to avoid the formation of thick resistive interphase layer.

2. Experimental Section

2.1. Materials Synthesis

The raw materials used were Li_2S (99.9%, Alfa Aesar), P_2S_5 (99%, Aladdin), and LiCl (99%, Aladdin). All the chemical reagents were used directly without further purification. All solid electrolytes were synthesized through the process of high-energy mechanical ball milling and following heat treatment. Typically, $Li_{5.5}PS_{4.5}Cl_{1.5}$ (LPSCl) electrolyte was synthesized by adding a stoichiometric of Li_2S, P_2S_5, and LiCl into a ball mill jar containing tungsten carbide grinding balls, then put jars into a planetary ball-milling apparatus (Pulverisette 7, Fritsch GmbH, Germany) at 450 rpm for 30 h. To ensure a uniform reaction of the powder, the jar should be removed from the apparatus to scrape the powder off the wall of the jar at intervals. After high-energy mechanical milling, the powder was heat-treated under vacuum at 550°C for 10 hours. $Li_{10}SnP_2S_{12}$ (LSPS) electrolyte was prepared by the same ball milling parameters at 450 rpm for 72 h and sintered at 550°C for 72 h. Synthesis of LGPS and $Li_7P_3S_{11}$ is supplemented in the Supporting Information. All sintered electrolytes were ground to powder and passed through a 300-mesh sieve before use.

To prepare the MIX electrolyte, the as-prepared LPSCl and LSPS powders were mixed with a desired mass ratio by hand grinding in an agate mortar for 10 min. The mass fraction of LSPS in the MIX electrolyte was controlled from 10 wt.% to 60 wt.%.

2.2. Preparation of lithium symmetric cells

The homemade battery molds were used to assemble the symmetric cells. 210 mg of solid electrolytes were pressed in a mold (13 mm in diameter) at 300 MPa for 10 min, then 100 μm thick lithium sheets were placed on both sides of the solid electrolyte pellets. A pressure of 7 MPa was maintained during the test.

2.3. Preparation of full cells

The cathode materials were made by ball milling $Li_4Ti_5O_{12}$, Ketjen black, and LPSCl at a mass ratio of 1:1:3 at 240 rpm for 6 h. The solid electrolyte powder was pressed at 75 MPa for 1 min, then spreading a certain amount of the cathode powder on one side of the solid electrolyte pellet and pressed at 300 MPa for 10 min. The mass loading of the active material was 1.4 mg cm^{-2}. Finally, a lithium foil was laid on the other side of the cell and a pressure of 7 MPa was maintained. The preparation procedure of NCM ($LiNiCoMnO_2$ (Ni:Co:Mn = 8:1:1)) full cell is supplemented in Supporting Information.

2.4. Materials Characterization

The crystallographic structures of the electrolytes were characterized by X-ray diffraction (XRD, Empyrean, PANalytical, Netherlands). XRD Rietveld refined samples were conducted at a step size of 0.02° with a dwell time of 4 seconds per step. Raman spectra were measured by a Raman spectrometer (in Via, Renishaw Inc., UK) using a 532 nm diode-pumped solid-state laser. The electrolyte samples for XRD and Raman spectra were sealed with a polyimide film to avoid humidity. The micromorphology of and the elemental distribution of the samples were detected by a field-emission scanning electron microscope (SEM, SU8010, Hitachi Inc., Japan) and an energy dispersive X-ray detector (EDX). Zview software was used to fit the experimental data. The interfacial chemistry within the cells was analyzed by an X-ray photoelectron spectroscopy device (XPS, ESCALAB 250Xi, Thermo Scientific Inc., US) with Al Kα-radiation.

2.5. Electrochemical Characterization

Galvanostatic charge−discharge tests of the cells were conducted using a Wuhan Land CT2001 battery tester. The electrochemical impedance spectra of lithium symmetric cells were measured by a frequency response analyzer (Solartron 1260A, Solartron Analytical Inc., UK). A perturbation voltage of 10 mV in the frequency range from 10^6 Hz to 1 Hz was applied. The electrochemical impedance spectra of full cells were measured at an electrochemical workstation (CHI660E, CHInstruments Ins., China) with a frequency range from 10^5 Hz to 0.01 Hz and a perturbation voltage of 10 mV.

3. Results and discussion

By mixing the two types of electrolytes, the MIX electrolyte is obtained. It is also possible to design the performance of the MIX electrolyte by adding a variety of electrolytes or organic and inorganic additives as what is done in conventional liquid electrolytes. Here, LPSCl and LSPS are chosen as the two electrolytes to be investigated in depth. If not specially mentioned, the MIX electrolyte with an optimized composition, 40 wt.% LSPS is discussed in the following.

To demonstrate the effectiveness of the mixed solid electrolyte, LPSCl is chosen as the Li-compatible component and LSPS as the dendrite-consuming component. The two solid electrolytes are uniformly mixed and then cold pressed at 300 MPa. As shown in the top-view SEM image in Fig. S2, the surface of the solid electrolyte pellet is relatively flat and has no obvious voids. This phenomenon is probably due to the similar Young's modulus of the two components [34]. It is not easy to distinguish the two different types of electrolytes from top-view SEM because the surface of the electrolyte sheet is too flat after cold pressing. Thus, the distribution of the two electrolytes particles is further shown by the cross-sectional SEM images (Fig.2a-c). Generally, the cross-sectional SEM image at low magnification (Fig. 2a) shows that the MIX electrolyte pellet is dense and free of cracks. The thickness of the MIX electrolyte is 0.9 mm. At higher magnification, it clearly shows two morphologically distinct regions, one exhibits a structure of tens of microns of large grains and the other exhibits an aggregated structure of several microns of small grains. The two kinds of regions are tightly pressed together, with no visible cracks and voids. EDX mapping (Fig. 2d) further confirms that the large grain regions are rich in Cl while the small particle regions are rich in Sn, indicating that the former is LPSCl, and the latter is LSPS. The two electrolytes are uniformly distributed at a scale of tens of microns. As a result of the impurity phase LiCl, it is also discovered that in LPSCl, there are some places that contain Cl but not S. To prove that the two electrolytes would not react after grinding, the reaction energy between LPSCl and LSPS is calculated by using the Materials Project [35, 36]. The reaction energy of the two electrolytes at any ratio is 0 eV/atom, which indicates that the interfaces of the two electrolytes are stable and do not react with each other at room temperature (Fig. S3).

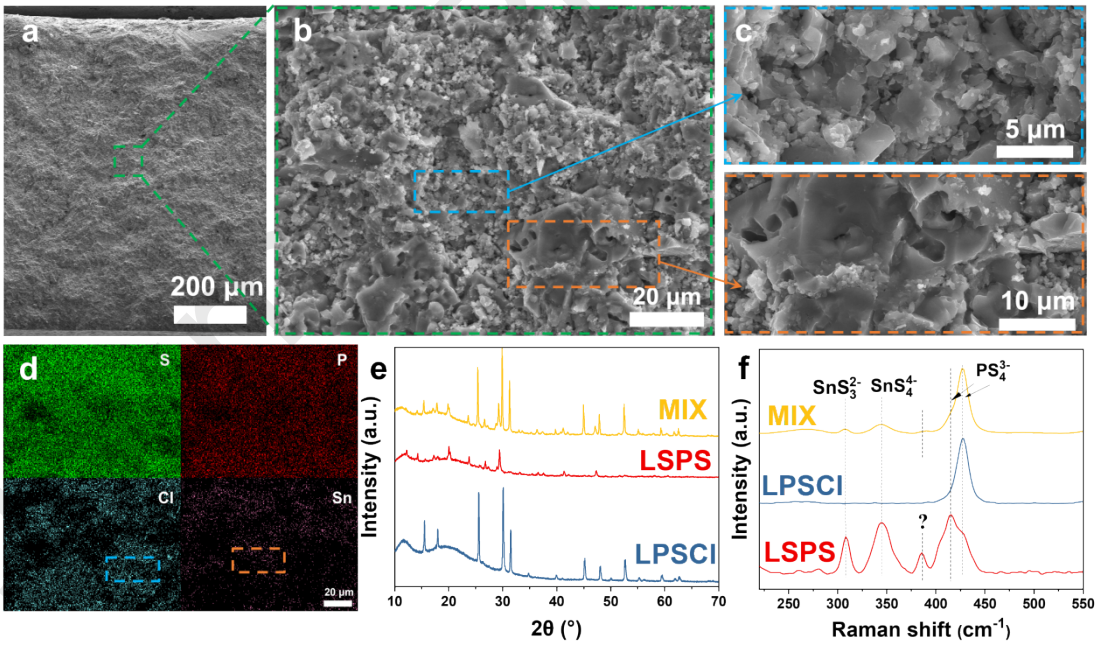

Figure 2. (a-c) cross-sectional SEM images of MIX electrolyte pellet at different magnifications. (d) EDX of the MIX electrolyte pellet. (e) Raman spectra of MIX, LPSCl, and LSPS. (f)XRD patterns of MIX, LSPS, and LPSCl.

According to XRD Rietveld refinement (Fig. S4), it is revealed that the as-

prepared LPSCl powder is mainly composed of an argyrodite phase (cubic, space group $F\bar{4}3m$), in accompany by 3.14 wt.% LiCl. The lattice parameter of the argyrodite phase is 9.788 Å, which is consistent with the study in the literature [13]. $Li_{5.5}PS_{4.5}Cl_{1.5}$, which has been utilized in this research, has a higher Cl doping level than Li_6PS_5Cl, increasing the Cl^-/S^{2-} site disorder and causing a stronger hetero-valent doping effect, allowing for higher ionic conductivity to be attained. The XRD Rietveld refinement also shows that the main structure of the as-prepared LSPS is $Li_{10}SnP_2S_{12}$ (tetragonal, space group $P4_2mc$ whose lattice parameters are $a = b = 8.74263$ Å, $c = 12.7701$ Å, $\alpha = \beta = \gamma = 90°$). Besides, there is 7.13 wt.% Li_2SnS_3 phase in the sample [37]. As shown in Figure 2e, the XRD pattern of the MIX electrolyte can be well reproduced by the superposition of those of the as-prepared LPSCl and LSPS. Thus, the two solid electrolytes are physically mixed in the MIX electrolyte.

Figure 2f shows the Raman spectra of the electrolyte powders in the wave number range of 200-550 cm^{-1}. In agreement with other reported LSPS results, the strongest Raman peaks at 422 cm^{-1} and 416 cm^{-1} are attributed to the PS_4 tetrahedron, and the peak at 346 cm^{-1} is attributed to the SnS_4 tetrahedron [38]. In addition, there is also an SnS_3 unit peak at 308 cm^{-1}, which is attributed to the impurity Li_2SnS_3 [39]. LPSCl exhibits the only peak at 422 cm^{-1} attributed to the PS_4 tetrahedron. Similarly, the Raman spectrum of the MIX electrolyte is the superposition of those of the as-prepared LPSCl and LSPS, further supporting the conclusion that the two solid electrolytes are mixed without chemical reactions.

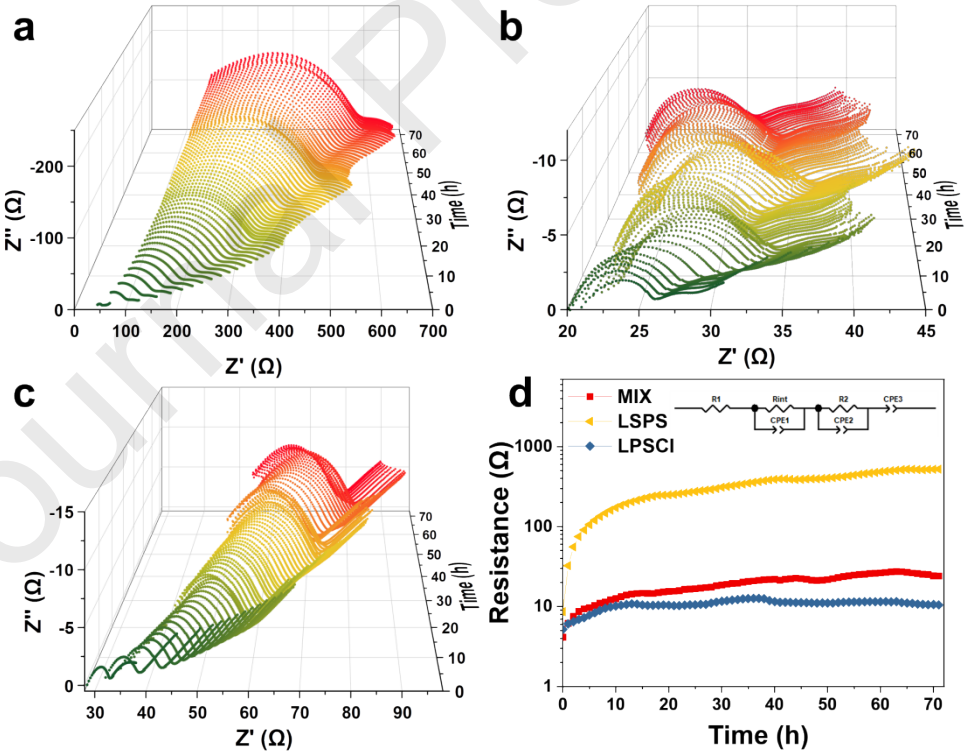

Figure 3. (a-c) The time-resolved impedance spectroscopy of LSPS, LPSCl, and MIX, from 0 to 72 h. (d) Evolution of the interfacial resistance of the Li symmetric cells.

The ionic conductivities of the as-prepared LPSCl and LSPS are 6.9 mS cm^{-1} and

2.4 mS cm^{-1}, respectively (Fig. S5). The MIX electrolyte exhibits an ionic conductivity of 3.6 mS cm^{-1}, which is between the ionic conductivities of the two components. The MIX electrolyte has an electronic conductivity of 3.9×10^{-9} S cm^{-1} also lies between the two components and does not become additionally large (Fig. S6). Conclusively, LPSCl and LSPS are physically and homogenously mixed at the micrometer scale, and the produced MIX electrolyte has a high ionic conductivity and a very low electronic conductivity, making it an appropriate solid-state electrolyte material for solid-state batteries.

Time-resolved impedance spectroscopy of the lithium symmetric cells is used to test the formation of the interphase layer between lithium and different solid electrolytes. As shown in Fig.3a-c, the impedance spectra of the three solid electrolytes shows different variation trends as monitored over 72 h. Periodical fluctuation of the spectra is caused by the slight environmental temperature difference between the day and the night. The equivalent circuit in the insert of Fig. 3d is used to fit the impedance spectra, so that the resistance of the interphase layer formed between lithium and the solid electrolytes can be deduced from the high-frequency semicircle (10^6-10^2 Hz) by the R_{int}-CPE1 element [40, 41]. As with the phenomena observed in other studies, a significant increase in the interphase layer resistance between Li and LSPS can be observed.[20] Differently, the interphase layer resistance increment for both LPSCl and MIX is relatively slow (Fig. 3d). For LSPS, The interphase layer resistance increases continually and reaches 500 Ω after 72 h. This effect is due to the fact that LSPS contains Sn^{4+}, which forms an MCI layer with high electronic conductivity when in contact with lithium metal [42]. The MCI layer does not effectively inhibit further reactions of Li to the electrolyte, resulting in an increasing resistance over time. In contrast, LPSCl and MIX are more stable with lithium. Their interphase layer resistance is less than 30 Ω even after 72 h. For MIX, the interphase layer resistance increases very slowly after several hours of stabilization, and for LPSCl, an even stable interphase layer resistance is observed benefiting from the formation of the electron-blocking SEI layer at the Li/LPSCl interface [24]. A suitable proportion of LPSCl within the MIX electrolyte significantly reduces the direct contact between LSPS and Li. The LSPS at some of the interfaces is inevitably decomposed into substances with considerable electronic conductivity. Fortunately, LPSCl in the MIX electrolyte, acting as a stable matrix, not only maintains the ion conduction path, but also guarantees a low effective electronic conductivity even when LSPS locally reacts with lithium. The MIX electrolyte delays the interfacial reaction between lithium and the solid electrolyte. Consequently, the MIX electrolyte, even containing LSPS, can exhibit a high level of lithium compatibility as long as a suitable ratio of LSPS to LPSCl is applied. These results illustrate that LSPS suffers severe interfacial reactions, while LPSCl and MIX retain good stability with Li metal.

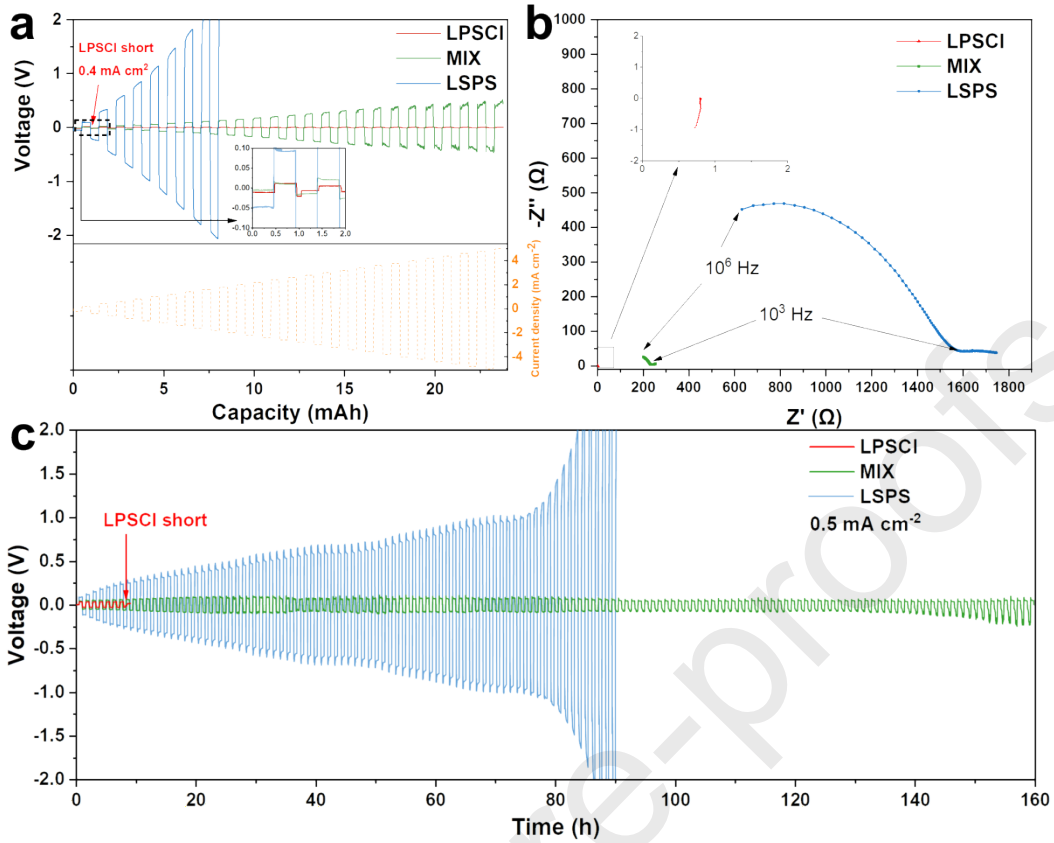

Figure 4. (a) Rate test of Li symmetric cells at step-increased current densities. The capacity of each charge and discharge process is 0.5 mAh cm^{-2}. (b) EIS of electrolytes after rate cycling. (c) Long-term cycle stability at 0.5 mA cm^{-2} current density with 0.25 mAh cm^{-2} areal capacity.

Lithium symmetric cells using LSPS, LPSCl, and MIX electrolyte are assembled, respectively. The rate performance of the symmetric lithium batteries is measured at step-increased current densities with an increment of 0.2 mA cm^{-2} per step. The capacity of each charging and discharging process is 0.5 mAh cm^{-2}. As shown in Fig.4a, the cell with LPSCl is shorted at 0.4 mA cm^{-2}, far from the high current densities required for the high-rate operation of all-solid-state batteries. The cell with LSPS shows severe polarization with the voltage exceeding 2 V when the current density is 1.6 mA cm^{-2}. This is due to the rapid reaction of the LSPS with the lithium when current is applied, rapidly forming MCI layers with great resistance and consequently increasing the polarization voltage. The battery can no longer be used owing to the huge overpotential. When the mass ratio of LSPS in the MIX is less than 30 wt.%, a soft short circuit occurs at high current density (Fig. S7a). When the mass ratio of LSPS in the MIX is more than 40 wt.%, the rapid increase of the overpotential can be observed once the current density is higher than 1.6 mA cm^{-2} (Fig. S7b). The mix ratio of the MIX electrolyte is optimized, and it is discovered that the MIX electrolyte with 40 wt.% LSPS can support a current density of 5.0 mA cm^{-2} without generating lithium penetration and can maintain a low overpotential of about 0.5 V at such a high current density (Fig. 4a). This is because when the LPSCl content is high complete short circuit is likely to occur at high currents, and when the LSPS content is high the severe reaction between LSPS and Li results in a very high polarization voltage. By adjusting the appropriate ratio of the two, an equilibrium can be achieved so that the cell is both short-circuit resistant and has a small polarization voltage at high currents. Therefore, without special

instruction, the MIX electrolyte discussed below is composed of 60 wt.% LPSCl and 40 wt.% LSPS.

Fig. 4b shows the electrochemical impedance spectrum (EIS) of the lithium symmetric cells after the rate-performance test. The EIS of the cell with LPSCl exhibits an inductance behavior, indicating that the cell is completely short-circuited. Differently, the EIS of the cell with LSPS shows a huge interphase layer resistance of 1591 Ω after the rate-performance test. Although for the cell with MIX, the interphase layer resistance also increases to 228 Ω, it is significantly smaller than the one with LSPS. To further study the origin of the increasing interphase layer resistance, the lithium symmetric cells after the rate-performance test are dissembled. The surface of the solid electrolytes in contact with Li can be exposed (Fig. S8). For the Li/LSPS/Li cell, the surface of the solid electrolyte is darkened and becomes rough. Moreover, the lithium electrodes are easily detached from the solid electrolyte, indicating a chemical-mechanical failure that leads to severe contact loss. For the Li/MIX/Li cell, the lithium electrodes still intimately adhere to the solid electrolyte, and after removing the lithium electrodes, the surface of the solid electrolyte shows only some black blemishes. The limited interfacial reaction between MIX and Li endows the Li/MIX/Li cell with much better cycling stability than the Li/LSPS/Li cell.

To further demonstrate the cycling stability of the MIX electrolyte, lithium plating/stripping cycling of the lithium symmetric cells is tested at a current density of 0.5 mA cm^{-2}. The LPSCl cell can only afford a few cycles and the cell is immediately short-circuited, while the voltage of the LSPS cell increase drastically and reaches a point where it can no longer be used after 90 h. After 90 h of cycling, the overpotential of the LSPS cell changes from 0.089 V to 5 V. The initial overpotentials of the LPSCl and MIX are 0.031 V and 0.039 V, respectively. However, at around 10 h the LPSCl cell short-circuits. Remarkably, the MIX cell has cycled steadily for 160 h while the overpotential increases from 0.043 V to 0.251 V, which is significantly less than the LSPS cell.

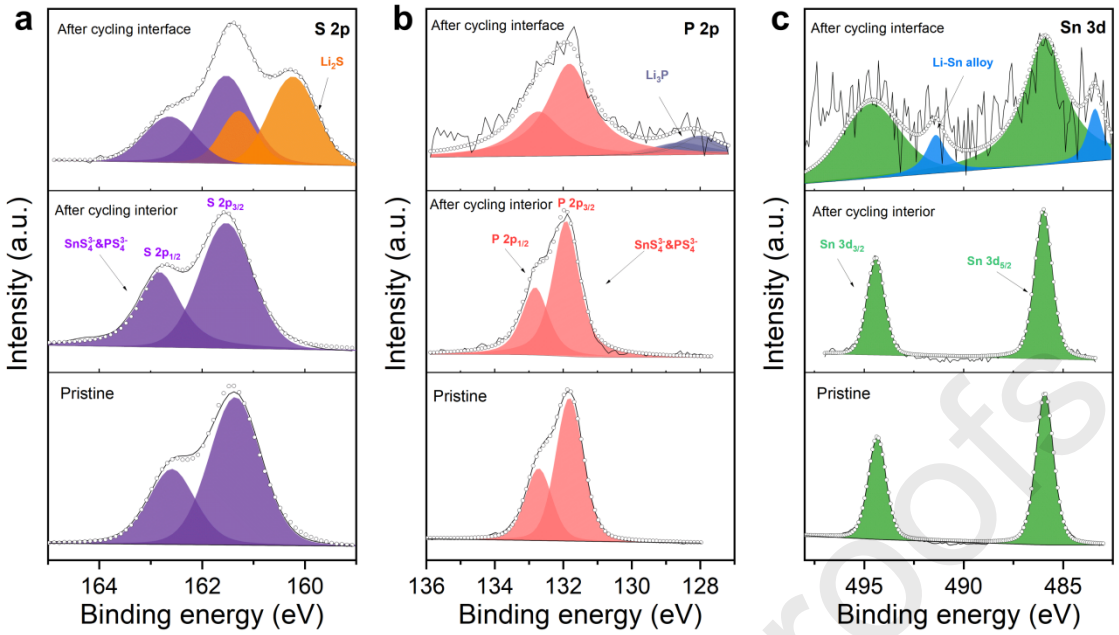

Figure 5 (a) S 2p, (b) P 2P and (c) Sn 3d XPS spectra of the MIX electrolyte collected from the interior and the MIX/Li interface. The spectra of the pristine electrolyte are also present for comparison.

The XPS results of the MIX electrolyte before and after the rate cycling are compared in order to further elucidate how the MIX electrolyte suppresses lithium dendrites and maintains a low interfacial resistance at the same time. The XPS spectra of Li 1s for these three samples show in Fig. S9a. All the Li 1s spectra show a Li-S peak at 55.4 eV and a Li-Cl peak at 56.1 eV. The Li-Cl peak corresponds to LPSCl inside the MIX electrolyte as well as some incompletely reacted LiCl [43]. For the spectra collected at the MIX/Li interface, an additional peak at 54.8 eV, attributed to Li^0, can be observed. It originates from the interfacial reaction product Li-Sn alloys as well as the Li adhering to the surface. As shown in Fig. 5a, the S 2p spectra collected from the interior of the MIX electrolyte do not change significantly before and after the cycling, showing a couple of peaks at 162.6 eV and 161.4 eV, which is attributed to SnS_4^{3-} and PS_4^{3-}. Differently, a couple of peaks attributed to Li_2S (161.3 eV and 160.2 eV) shows up in the spectrum collected at the MIX/Li interface after cycling, signifying an evident lithiation of the MIX electrolyte [44]. This indicates that in the MIX electrolyte, the decomposition mainly occurs at the interface, and is well suppressed within the electrolyte. Similar conclusions can be drawn from the P 2p spectra (Fig. 5b). The pristine spectrum shows a couple of P 2p peaks at 132.6 eV and 131.8 eV, attributed to SnS_4^{3-} and PS_4^{3-}. After cycling, the spectrum collected from the interior shows almost the same signals, while the one collected at the interface shows additional peaks at 128.6 eV and 127.9 eV, which correspond to the electrolyte decomposition product Li_3P. The Sn 3d spectra (Fig. 5c) shows the signals of Sn^{4+} in LSPS at 494.4 eV and 485.9 eV. As for Sn 3d spectrum collected at the interface after cycling, the peak intensity decreases significantly. Moreover, there appear additional peaks associated with Li-Sn alloy at 491.7 eV and 483.5 eV, indicating that the LSPS has partially decomposed at the MIX/Li interface [17]. The XPS fine sweep spectra of Cl (Fig. S9b) is unchanged after cycling, whether collected from the interior or at the interface, showing the good stability of LPSCl [45]. According to the XPS results, it can be confirmed that after rate cycling, the decomposition of LSPS is almost confined

near the MIX/Li interface. This limited decomposition of LSPS, in one aspect, consumes the lithium dendrites generated at high currents, and in the other aspect, avoids the continuous growth of the highly resistive interphase layer.

After rate cycling, the MIX electrolyte was homogeneously ground and subjected to XRD. It is clear to see that the peak intensity of the sample after the rate cycling decreases to some extent, though with no obvious peaks of new compounds generated (Fig. S10). The SEM of the interface after the rate cycling (Fig. S11) also shows that it becomes slightly loose. Combined with the above observations, we infer that there is a significant reaction at the electrolyte interface and that the internal electrolyte maintains its normal performance. This indicates that the electrolyte still has good electrochemical properties after the reaction induced by the high-current cycling. In principle, the MIX electrolyte can be prepared by mixing a lithium-metastable solid electrolyte and a lithium-unstable solid electrolyte, where the former acts as a lithium-compatible matrix, and the latter as a dendrite-scavenger. To demonstrate the university of this strategy, another combination, $Li_7P_3S_{11}$ and $Li_{10}GeP_2S_{12}$ are chosen to prepare the MIX electrolyte. The mass ratio between $Li_7P_3S_{11}$ and $Li_{10}GeP_2S_{12}$ is 60:40. The rate test of the lithium symmetric cells is presented in Fig. S12. It shows that this modified combination can also afford a high current density of up to 5 mA cm^{-2} without a short circuit.

Finally, full batteries are assembled to evaluate the electrochemical performance of the MIX electrolyte. Here, LTO is used as the active material of the cathode, lithium metal as the anode and the MIX electrolyte as the separator. LTO exhibits excellent cycling stability. Moreover, it is compatible with sulfide solid electrolytes, so that the side reactions in the cathode could be avoided [46-48]. To further reduce the side reactions, the voltage window is adjusted to 1.3 - 2.3 V. In this voltage range, the decomposition of the solid electrolyte is significantly suppressed [44, 49]. For comparison, ASSLMBs with electrolytes of LPSCl and LSPS are also prepared using the same manufacturing process. The rate-performance tests show that at 0.2 C rate, the batteries with LSPS and with MIX have a high initial capacity of 180 mAh g^{-1} and 174 mAh g^{-1}, respectively, whereas the one with LPSCl has a relatively low capacity of 139 mAh g^{-1}. Typically, the sulfide solid electrolytes containing metal elements, like LSPS and LGPS, tend to provide a certain amount of battery capacity, owing to their poorer stability than other sulfide solid electrolytes[50]. Once the rate increases, the battery with LPSCl quickly short circuits at 0.5 C, which is reflected by the fluctuating charge curve and the much higher charge capacity than the discharge capacity (Fig. 6f). This corresponds to the low CCD of LPSCl as revealed in the Li symmetric cell (Fig. 4a). As for the battery with LSPS, the rate capacities are 167 mAh g^{-1}, 133 mAh g^{-1}, and 20 mAh g^{-1}at 0.5, 1, and 2 C rates, respectively. The drastic capacity degradation at 2 C is ascribed to the extremely large overpotential (Fig. 6e). The catastrophic polarization at a high rate is ameliorated in the battery with the MIX electrolyte, whose rate capacities are 164 mAh g^{-1}, 159 mAh g^{-1}, and 148 mAh g^{-1} at 0.5, 1, and 2 C rates, respectively. Moreover, no short circuit occurs even at a 2 C rate when the MIX electrolyte is used. During 1 C rate cycling, the overpotential of the batteries, measured at half of the theoretical capacity, is 0.050 V, and 0.220V for MIX and LSPS, respectively. Since LPSCl is short-circuited at 1 C, its overpotential is 0.032 V at 0.5 C. The much higher overpotential of the LSPS battery is associated with the high interphase layer resistance, which will be discussed below by the EIS results. Fig. 6a also shows that all three batteries have a coulombic efficiency greater than 100% in the initial few cycles. This

may be related to the side reactions between the electrolyte and the lithium anode. With the increase of cycle numbers, coulombic efficiency all converges to 100%. It is also tested with a commercial NCM-811 cathode material and maintained 77% capacity after 150 cycles of 2 C (Fig. S13), with no short circuit occurring.

The EIS of the batteries before and after the rate test is shown in Fig. 5b-c. The incomplete high-frequency semicircle (10^5-10^2 Hz) is associated with the interphase layer formed between the lithium and the solid electrolyte, the medium frequency (10^2-1 Hz) semicircle with the charge transfer process of the lithium anode, and the low frequency (1-0.01Hz) segment with the diffusion process of the lithium in the cathode. Before the rate test, the batteries with LPSCl and MIX have similar EIS, with both showing an interphase layer resistance of less than 10 Ω. Differently, the interphase layer resistance of the LSPS battery is 70 Ω. After the rate test, the impedance of the LPSCl battery slightly decreases, which corresponds to the soft short circuit of the battery. A different case is observed in the LSPS battery, where the interphase layer resistance drastically increases to 400 Ω, indicating the battery underwent violent interfacial reactions during the cycling. In contrast, the MIX maintains a relatively small interphase layer resistance of 84 Ω after the rate test. EIS results indicate that the huge overpotential of the LSPS battery is principally ascribed to the uncontrollable growth of the interphase layer between LSPS and the lithium anode, and the MIX electrolyte can effectively inhibit interfacial reactions benefitting from the good stability of LPSCl to lithium. To further test the cycling stability of the batteries using the MIX electrolyte, galvanostatic charge/discharge is carried out at 1 C and 2 C, respectively. As can be seen in Fig. 5g, the batteries exhibit excellent cycling stability, retaining 94.4% and 97.3% capacity after 75 cycles at 1 C and 2 C, respectively, and keep nearly 100% coulombic efficiency. This excellent stability and high coulombic efficiency indicate that the MIX electrolyte can effectively stabilize the lithium/solid electrolyte interface and can inhibit the short circuit of the ASSLMBs.

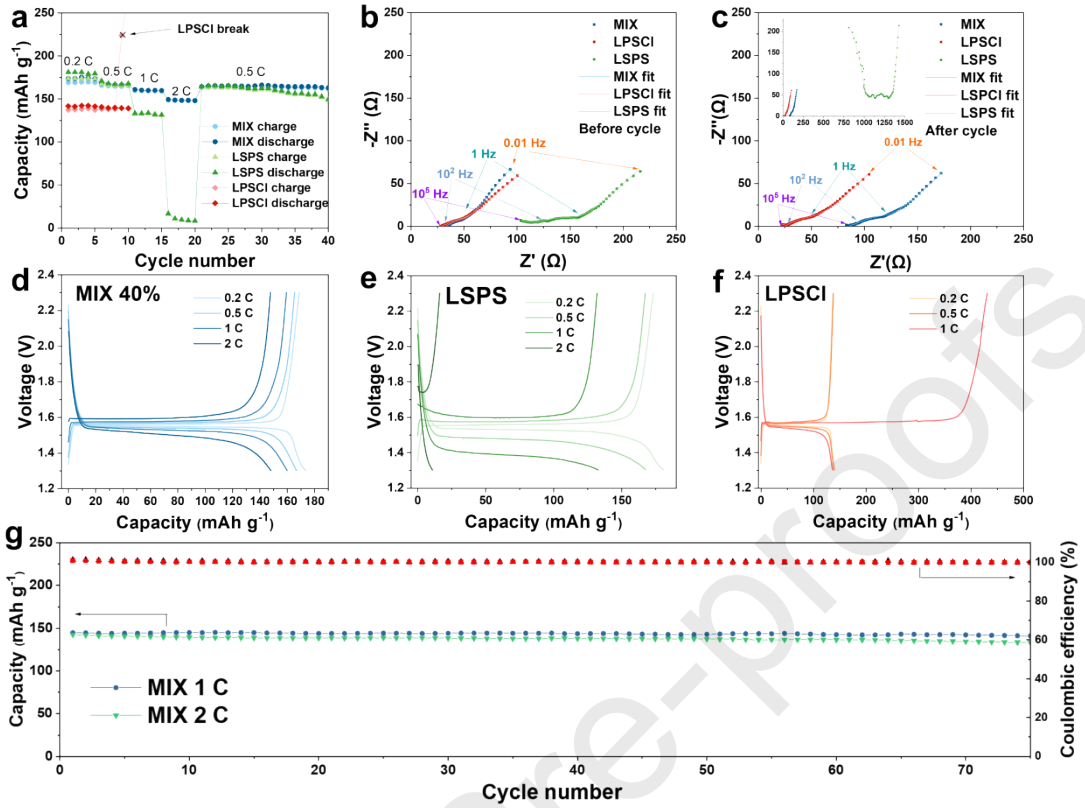

Figure 6. (a) Rate performance of Li/SEs/LTO ASSLMBs (SEs = MIX, LSPS, LPSCl). (b-c) Nyquist plots of Li/SEs/Li ASSLMBs before and after cycling. (d-f) Charge/discharge profiles of ASSLMBs. (g) Cycling performances of the Li/MIX /LTO ASSLMB at 1 C and 2 C.

4. Conclusions

In summary, the mixed solid electrolyte is prepared from two different types of SEs by a simple mixing strategy, one of which efficiently consumes lithium dendrites, and the other is meta-stable with Li anode. The MIX solid electrolyte exhibits good Li-compatibility and excellent lithium-dendrite resistance. Using this MIX electrolyte, the Li symmetric cells are found to operate stably for 160 h at 0.5 mA cm^{-2} without a short circuit. Even at a current density of 5 mA cm^{-2}, the overpotential is lower than 0.5 V. The Li/SEs/LTO ASSLMBs are prepared and exhibit a high capacity of 174 mAh g^{-1} at 0.2 C and 148 mAh g^{-1} at 2 C, showing excellent rate performance. High-capacity retention of 97.3% and 94.4% are shown after 75 cycles at room temperature at 1 C and 2 C, respectively. The high adaptability of MIX solid electrolyte may make it possible to use not just two electrolytes with different properties, but even three or more electrolytes and additives with varied properties to specifically optimize the performance of the all-solid-state battery. This simple preparation method provides a completely new idea for developing novel solid electrolytes in order to meet the requirements of the commercialization of all-solid-state batteries.

Supporting Information.

The support information is available free of charge.

Acknowledgment

This work is financially supported by the Natural Science Foundation of Guangdong Province (No. 2021A1515011725), and the Shenzhen Science and Technology Foundation (JCYJ20210324095808023).

CRediT authorship contribution statement

Zeyu Ge: Conceptualization, Methodology, Validation, Investigation, Writing – original draft. **Nanshan Chen**: Conceptualization, Validation, Investigation, Writing – original draft. **Rui Wang**: Investigation, Validation, Writing – review & editing. **Rui Ma**: Methodology, Investigation, Writing – review & editing. **Fan Bo**: Methodology, Investigation, Writing – review & editing. **David Le coq**: Methodology, Investigation, Writing – review & editing. **Xianghua Zhang**: Methodology, Investigation, Writing – review & editing. **Hongli Ma**: Methodology, Investigation, Writing – review & editing. **Bai Xue**: Conceptualization, Methodology, Validation, Investigation, Writing – original draft, Writing – review & editing, Supervision, Project administration.

Zeyu Ge and **Nanshan Chen** contributed equally to this work as co-first authors.

Conflict of Interest

There are no conflicts to declare.

[1] F. Duffner, N. Kronemeyer, J. Tübke, J. Leker, M. Winter, R. Schmuch, Post-lithium-ion battery cell production and its compatibility with lithium-ion cell production infrastructure, Nature Energy 6(2) (2021) 123-134. https://doi.org/10.1038/s41560-020-00748-8.

[2] L.-Z. Fan, H. He, C.-W. Nan, Tailoring inorganic–polymer composites for the mass production of solid-state batteries, Nature Reviews Materials 6(11) (2021) 1003-1019. https://doi.org/10.1038/s41578-021-00320-0.

[3] Y. Chen, Z. Wang, X. Li, X. Yao, C. Wang, Y. Li, W. Xue, D. Yu, S.Y. Kim, F. Yang, A. Kushima, G. Zhang, H. Huang, N. Wu, Y.W. Mai, J.B. Goodenough, J. Li, Li metal deposition and stripping in a solid-state battery via Coble creep, Nature 578(7794) (2020) 251-255. https://doi.org/10.1038/s41586-020-1972-y.

[4] D. Lin, Y. Liu, Y. Cui, Reviving the lithium metal anode for high-energy batteries, Nat Nanotechnol 12(3) (2017) 194-206. https://doi.org/10.1038/nnano.2017.16.

[5] J. Janek, W.G. Zeier, A solid future for battery development, Nature Energy 1(9) (2016) 16141. https://doi.org/10.1038/Nenergy.2016.141.

[6] B.S. Vishnugopi, E. Kazyak, J.A. Lewis, J. Nanda, M.T. McDowell, N.P. Dasgupta, P.P. Mukherjee, Challenges and Opportunities for Fast Charging of Solid-State Lithium Metal Batteries, ACS Energy Letters 6(10) (2021) 3734-3749. https://doi.org/10.1021/acsenergylett.1c01352.

[7] Y. Qian, K. Zhang, L. Tan, Y. An, B. Xi, S. Xiong, J. Feng, Y. Qian, Highly reversible and safe lithium metal batteries enabled by Non-flammable All-fluorinated carbonate electrolyte conjugated with 3D flexible MXene-based lithium anode, Chemical Engineering Journal 440 (2022). https://doi.org/10.1016/j.cej.2022.135818.

[8] S. Sarkar, V. Thangadurai, Critical Current Densities for High-Performance All-Solid-State Li-Metal Batteries: Fundamentals, Mechanisms, Interfaces, Materials, and Applications, ACS Energy Letters 7(4) (2022) 1492-1527. https://doi.org/10.1021/acsenergylett.2c00003.

[9] W. Lu, M. Xue, C. Zhang, Modified Li7La3Zr2O12 (LLZO) and LLZO-polymer composites for solid-state lithium batteries, Energy Storage Materials 39 (2021) 108-129. https://doi.org/10.1016/j.ensm.2021.04.016.

[10] Z. Zhao, Z. Wen, X. Liu, H. Yang, S. Chen, C. Li, H. Lv, F. Wu, B. Wu, D. Mu, Tuning a compatible interface with LLZTO integrated on cathode material for improving NCM811/LLZTO solid-state battery, Chemical Engineering Journal 405 (2021) 127031. https://doi.org/10.1016/j.cej.2020.127031.

[11] F. Shen, M.B. Dixit, X. Xiao, K.B. Hatzell, Effect of Pore Connectivity on Li Dendrite Propagation within LLZO Electrolytes Observed with Synchrotron X-ray Tomography, ACS Energy Letters 3(4) (2018) 1056-1061. https://doi.org/10.1021/acsenergylett.8b00249.

[12] C. Wang, J. Liang, Y. Zhao, M. Zheng, X. Li, X. Sun, All-solid-state lithium batteries enabled by sulfide electrolytes: from fundamental research to practical engineering design, Energy & Environmental Science 14(5) (2021) 2577-2619.

https://doi.org/10.1039/d1ee00551k.

[13] P. Adeli, J.D. Bazak, K.H. Park, I. Kochetkov, A. Huq, G.R. Goward, L.F. Nazar, Boosting Solid-State Diffusivity and Conductivity in Lithium Superionic Argyrodites by Halide Substitution, Angew Chem Int Ed Engl 58(26) (2019) 8681-8686. https://doi.org/10.1002/anie.201814222.

[14] D. Zeng, J. Yao, L. Zhang, R. Xu, S. Wang, X. Yan, C. Yu, L. Wang, Promoting favorable interfacial properties in lithium-based batteries using chlorine-rich sulfide inorganic solid-state electrolytes, Nat Commun 13(1) (2022) 1909. https://doi.org/10.1038/s41467-022-29596-8.

[15] T. Krauskopf, F.H. Richter, W.G. Zeier, J. Janek, Physicochemical Concepts of the Lithium Metal Anode in Solid-State Batteries, Chem Rev 120(15) (2020) 7745-7794. https://doi.org/10.1021/acs.chemrev.0c00431.

[16] S.P. Ong, Y. Mo, W.D. Richards, L. Miara, H.S. Lee, G. Ceder, Phase stability, electrochemical stability and ionic conductivity of the Li10±1MP2X12(M = Ge, Si, Sn, Al or P, and X = O, S or Se) family of superionic conductors, Energy Environ. Sci. 6(1) (2013) 148-156. https://doi.org/10.1039/c2ee23355j.

[17] B.Z. Zheng, X.S. Liu, J.P. Zhu, J. Zhao, G.M. Zhong, Y.X. Xiang, H.C. Wang, W.M. Zhao, E. Umeshbabu, Q.H. Wu, J.Y. Huang, Y. Yang, Unraveling (electro)-chemical stability and interfacial reactions of Li10SnP2S12 in all-solid-state Li batteries, Nano Energy 67 (2020) 104252. https://doi.org/10.1016/j.nanoen.2019.104252.

[18] W. Fitzhugh, X. Chen, Y. Wang, L. Ye, X. Li, Solid–electrolyte-interphase design in constrained ensemble for solid-state batteries, Energy & Environmental Science 14(8) (2021) 4574-4583. https://doi.org/10.1039/d1ee00754h.

[19] N. Kamaya, K. Homma, Y. Yamakawa, M. Hirayama, R. Kanno, M. Yonemura, T. Kamiyama, Y. Kato, S. Hama, K. Kawamoto, A. Mitsui, A lithium superionic conductor, Nat Mater 10(9) (2011) 682-6. https://doi.org/10.1038/nmat3066.

[20] S. Wenzel, S. Randau, T. Leichtweiß, D.A. Weber, J. Sann, W.G. Zeier, J. Janek, Direct Observation of the Interfacial Instability of the Fast Ionic Conductor Li10GeP2S12 at the Lithium Metal Anode, Chemistry of Materials 28(7) (2016) 2400-2407. https://doi.org/10.1021/acs.chemmater.6b00610.

[21] H. Pan, M. Zhang, Z. Cheng, H. Jiang, J. Yang, P. Wang, P. He, H. Zhou, Carbon-free and binder-free Li-Al alloy anode enabling an all-solid-state Li-S battery with high energy and stability, Science Advances 8(15) (2022) eabn4372. https://doi.org/doi:10.1126/sciadv.abn4372.

[22] S. Luo, Z. Wang, X. Li, X. Liu, H. Wang, W. Ma, L. Zhang, L. Zhu, X. Zhang, Growth of lithium-indium dendrites in all-solid-state lithium-based batteries with sulfide electrolytes, Nat Commun 12(1) (2021) 6968. https://doi.org/10.1038/s41467-021-27311-7.

[23] J.M. Doux, H. Nguyen, D.H.S. Tan, A. Banerjee, X. Wang, E.A. Wu, C. Jo, H. Yang, Y.S. Meng, Stack Pressure Considerations for Room-Temperature

All-Solid-State Lithium Metal Batteries, Advanced Energy Materials 10(1) (2019) 1903253. https://doi.org/10.1002/aenm.201903253.

[24] C. Lee, S.Y. Han, J.A. Lewis, P.P. Shetty, D. Yeh, Y. Liu, E. Klein, H.-W. Lee, M.T. McDowell, Stack Pressure Measurements to Probe the Evolution of the Lithium–Solid-State Electrolyte Interface, ACS Energy Letters 6(9) (2021) 3261-3269. https://doi.org/10.1021/acsenergylett.1c01395.

[25] Z. Ning, D.S. Jolly, G. Li, R. De Meyere, S.D. Pu, Y. Chen, J. Kasemchainan, J. Ihli, C. Gong, B. Liu, D.L.R. Melvin, A. Bonnin, O. Magdysyuk, P. Adamson, G.O. Hartley, C.W. Monroe, T.J. Marrow, P.G. Bruce, Visualizing plating-induced cracking in lithium-anode solid-electrolyte cells, Nat Mater 20(8) (2021) 1121-1129. https://doi.org/10.1038/s41563-021-00967-8.

[26] J.A. Lewis, F.J.Q. Cortes, Y. Liu, J.C. Miers, A. Verma, B.S. Vishnugopi, J. Tippens, D. Prakash, T.S. Marchese, S.Y. Han, C. Lee, P.P. Shetty, H.W. Lee, P. Shevchenko, F. De Carlo, C. Saldana, P.P. Mukherjee, M.T. McDowell, Linking void and interphase evolution to electrochemistry in solid-state batteries using operando X-ray tomography, Nat Mater 20(4) (2021) 503-510. https://doi.org/10.1038/s41563-020-00903-2.

[27] C. Wang, Y. Zhao, Q. Sun, X. Li, Y. Liu, J. Liang, X. Li, X. Lin, R. Li, K.R. Adair, L. Zhang, R. Yang, S. Lu, X. Sun, Stabilizing interface between Li10SnP2S12 and Li metal by molecular layer deposition, Nano Energy 53 (2018) 168-174. https://doi.org/10.1016/j.nanoen.2018.08.030.

[28] H. Wan, S. Liu, T. Deng, J. Xu, J. Zhang, X. He, X. Ji, X. Yao, C. Wang, Bifunctional Interphase-Enabled Li10GeP2S12 Electrolytes for Lithium–Sulfur Battery, ACS Energy Letters 6(3) (2021) 862-868. https://doi.org/10.1021/acsenergylett.0c02617.

[29] X. Wu, S. Cui, M. Fei, S. Liu, X. Gao, G. Li, Inverse-opal structured TiO2 regulating electrodeposition behavior to enable stable lithium metal electrodes, Green Energy & Environment (2022). https://doi.org/10.1016/j.gee.2022.03.010.

[30] J. Xu, J. Li, Y. Li, M. Yang, L. Chen, H. Li, F. Wu, Long-Life Lithium-Metal All-Solid-State Batteries and Stable Li Plating Enabled by In Situ Formation of Li(3) PS(4) in the SEI Layer, Adv Mater 34(34) (2022) e2203281. https://doi.org/10.1002/adma.202203281.

[31] X. Li, D. Wang, H. Wang, H. Yan, Z. Gong, Y. Yang, Poly(ethylene oxide)-Li(10)SnP(2)S(12) Composite Polymer Electrolyte Enables High-Performance All-Solid-State Lithium Sulfur Battery, ACS Appl Mater Interfaces 11(25) (2019) 22745-22753. https://doi.org/10.1021/acsami.9b05212.

[32] Z. Wang, Y. Zhang, P. Zhang, D. Yan, J. Liu, Y. Chen, Q. Liu, P. Cheng, M.J. Zaworotko, Z. Zhang, Thermally rearranged covalent organic framework with flame-retardancy as a high safety Li-ion solid electrolyte, eScience 2(3) (2022) 311-318. https://doi.org/10.1016/j.esci.2022.03.004.

[33] H. Yang, B. Zhang, M. Jing, X. Shen, L. Wang, H. Xu, X. Yan, X. He, In Situ

Catalytic Polymerization of a Highly Homogeneous PDOL Composite Electrolyte for Long-Cycle High-Voltage Solid-State Lithium Batteries, Advanced Energy Materials 12(39) (2022) 2201762. https://doi.org/10.1002/aenm.202201762.

[34] Q. Zhang, D. Cao, Y. Ma, A. Natan, P. Aurora, H. Zhu, Sulfide-Based Solid-State Electrolytes: Synthesis, Stability, and Potential for All-Solid-State Batteries, Adv Mater 31(44) (2019) e1901131. https://doi.org/10.1002/adma.201901131.

[35] A. Jain, S.P. Ong, G. Hautier, W. Chen, W.D. Richards, S. Dacek, S. Cholia, D. Gunter, D. Skinner, G. Ceder, K.A. Persson, Commentary: The Materials Project: A materials genome approach to accelerating materials innovation, Apl Materials 1(1) (2013) 011002. https://doi.org/10.1063/1.4812323.

[36] Y. Wang, L. Ye, X. Chen, X. Li, A Two-Parameter Space to Tune Solid Electrolytes for Lithium Dendrite Constriction, JACS Au 2(4) (2022) 886-897. https://doi.org/10.1021/jacsau.2c00009.

[37] Q. Wang, D. Liu, X. Ma, X. Zhou, Z. Lei, Cl-Doped Li(10)SnP(2)S(12) with Enhanced Ionic Conductivity and Lower Li-Ion Migration Barrier, ACS Appl Mater Interfaces 14(19) (2022) 22225-22232. https://doi.org/10.1021/acsami.2c05203.

[38] H. Wang, L. Wu, B. Xue, F. Wang, Z. Luo, X. Zhang, L. Calvez, P. Fan, B. Fan, Improving Cycling Stability of the Lithium Anode by a Spin-Coated High-Purity Li(3)PS(4) Artificial SEI Layer, ACS Appl Mater Interfaces 14(13) (2022) 15214-15224. https://doi.org/10.1021/acsami.1c25224.

[39] P. Bron, S. Johansson, K. Zick, J. Schmedt auf der Gunne, S. Dehnen, B. Roling, Li10SnP2S12: an affordable lithium superionic conductor, J Am Chem Soc 135(42) (2013) 15694-7. https://doi.org/10.1021/ja407393y.

[40] B. Fan, Z.B. Guan, H.J. Wang, L.L. Wu, W.Z. Li, S.B. Zhang, B. Xue, Electrochemical processes in all-solid-state Li-S batteries studied by electrochemical impedance spectroscopy, Solid State Ionics 368 (2021) 115680. https://doi.org/10.1016/j.ssi.2021.115680.

[41] H.L. Li, T. Zhang, Z. Yang, Y.L. Shi, Q.C. Zhuang, Y.H. Cui, Electrochemical Impedance Spectroscopy Study on Using Li10GeP2S12 Electrolyte for All-Solid-State Lithium Batteries, International Journal of Electrochemical Science 16(2) (2021) 210229. https://doi.org/10.20964/2021.02.33.

[42] I. Tarhouchi, V. Viallet, P. Vinatier, M. Ménétrier, Electrochemical characterization of Li10SnP2S12: An electrolyte or a negative electrode for solid state Li-ion batteries?, Solid State Ionics 296 (2016) 18-25. https://doi.org/10.1016/j.ssi.2016.08.016.

[43] A.L. Davis, E. Kazyak, D.W. Liao, K.N. Wood, N.P. Dasgupta, Operando Analysis of Interphase Dynamics in Anode-Free Solid-State Batteries with Sulfide Electrolytes, Journal of The Electrochemical Society 168(7) (2021) 070557. https://doi.org/10.1149/1945-7111/ac163d.

[44] D.H.S. Tan, E.A. Wu, H. Nguyen, Z. Chen, M.A.T. Marple, J.-M. Doux, X. Wang, H. Yang, A. Banerjee, Y.S. Meng, Elucidating Reversible Electrochemical Redox of

Li6PS5Cl Solid Electrolyte, ACS Energy Letters 4(10) (2019) 2418-2427. https://doi.org/10.1021/acsenergylett.9b01693.

[45] J. Auvergniot, A. Cassel, D. Foix, V. Viallet, V. Seznec, R. Dedryvère, Redox activity of argyrodite Li6PS5Cl electrolyte in all-solid-state Li-ion battery: An XPS study, Solid State Ionics 300 (2017) 78-85. https://doi.org/10.1016/j.ssi.2016.11.029.

[46] G.-L. Zhu, C.-Z. Zhao, H. Yuan, B.-C. Zhao, L.-P. Hou, X.-B. Cheng, H.-X. Nan, Y. Lu, J. Zhang, J.-Q. Huang, Q.-B. Liu, C.-X. He, Q. Zhang, Interfacial redox behaviors of sulfide electrolytes in fast-charging all-solid-state lithium metal batteries, Energy Storage Materials 31 (2020) 267-273. https://doi.org/10.1016/j.ensm.2020.05.017.

[47] L. Feng, Z.W. Yin, C.W. Wang, Z. Li, S.J. Zhang, P.F. Zhang, Y.P. Deng, F. Pan, B. Zhang, Z. Lin, Glassy/Ceramic Li2TiO3/LixByOz Analogous "Solid Electrolyte Interphase" to Boost 4.5 V LiCoO2 in Sulfide-Based All-Solid-State Batteries, Advanced Functional Materials (2023) 2210744. https://doi.org/10.1002/adfm.202210744.

[48] C.-W. Wang, F.-C. Ren, Y. Zhou, P.-F. Yan, X.-D. Zhou, S.-J. Zhang, W. Liu, W.-D. Zhang, M.-H. Zou, L.-Y. Zeng, X.-Y. Yao, L. Huang, J.-T. Li, S.-G. Sun, Engineering the interface between LiCoO2 and Li10GeP2S12 solid electrolytes with an ultrathin Li2CoTi3O8 interlayer to boost the performance of all-solid-state batteries, Energy & Environmental Science 14(1) (2021) 437-450. https://doi.org/10.1039/d0ee03212c.

[49] C.-W. Wang, S.-J. Zhang, C. Lin, S. Xue, Y.-P. Deng, B. Zhang, L. Yang, X. Yao, L. Zeng, J.-T. Li, F. Pan, Z.-W. Yin, Mechanochemical reactions between polyanionic borate and residue Li2CO3 on LiCoO2 to stabilize cathode/electrolyte interface in sulfide-based all-solid-state batteries, Nano Energy 108 (2023) 108192. https://doi.org/10.1016/j.nanoen.2023.108192.

[50] F. Han, T. Gao, Y. Zhu, K.J. Gaskell, C. Wang, A Battery Made from a Single Material, Adv Mater 27(23) (2015) 3473-83. https://doi.org/10.1002/adma.201500180.

Highlights：

1. High-performance solid electrolytes are prepared by simple hand-mixing.

2. The solid electrolytes can stand 5 mA cm^{-2} without lithium penetration.

3. The overpotential of symmetric lithium cells is less than 0.5 V at 5 mA cm^{-2}.

4. The Li/SE/$Li_4Ti_5O_{12}$ cells show 94.4% capacity retention after 75 cycles at 2 C.

1